Synthetic functional π-stack architecture in lipid bilayers

Sheshanath Bhosale, Adam L. Sisson, Naomi Sakai and Stefan Matile*

Received 9th May 2006, Accepted 13th June 2006
First published as an Advance Article on the web 7th July 2006
DOI: 10.1039/b606487f

Neglected until recently, π-stack architecture is rapidly emerging as a powerful strategy to create function in lipid bilayer membranes. Recent reports describe supramolecular rosettes acting as hosts of intercalating guests, to assemble in bilayer membranes and, in the case of stacked guanosine and folate quartets, to form ion channels. The introduction of rigid-rod π-stack architecture allowed us to address one of the great challenges in the field, *i.e.* ligand gating. Inspiring π-stack chemistry from related fields, covering rainbow coloration, conductivity, as well as the critical dependence of charge mobilities on the precision of supramolecular organization is summarized to zoom in on arguably the most promising application of functional π-stack architecture in lipid bilayers, that is the creation of multifunctional photosystems.

1 Introduction

Functional π-stack architecture plays a central role in the chemistry and biology of oligonucleotides. The same motif is, however, surprisingly rare in biomolecules that function in lipid bilayer membranes. Transmembrane co-facial π-stack architecture beyond the special pair of chlorophylls contributes, for instance, surprisingly little to the structure and function of biological photosystems, not to speak of biological ion channels or pores.[1–3] Quite the same is true for synthetic photosystems, ion channels and pores.[4–7] The only synthetic route to multifunctional pores available today, for example, uses about 150 hydrogen bonds for the non-covalent transformation of rigid-rod molecules **1** into rigid-rod β-barrels **2** (Fig. 1).[8]

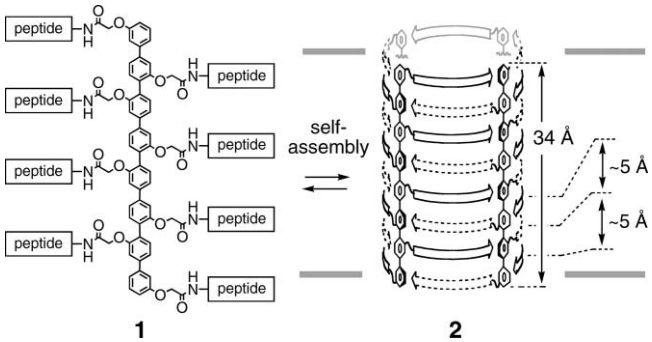

Fig. 1 Self-assembly of synthetic multifunctional pores **2** from rigid-rod molecules **1**.

Department of Organic Chemistry, University of Geneva, Geneva, Switzerland. E-mail: stefan.matile@chiorg.unige.ch; Fax: +41 22 379 5123; Tel: +41 22 379 6523

Now, however, this situation is changing. Transmembrane π-stack architecture is rapidly emerging as an attractive strategy to

From left to right: Sheshanath Bhosale, Adam Sisson, Naomi Sakai and Stefan Matile

Sheshanath Bhosale received his MSc from SRTM University, Nanded, India. He obtained his PhD from the Freie University Berlin, Germany, in 2004 for research in supramolecular chemistry with Professor Jurgen-Hinrich Fuhrhop. Currently, he is a post-doctoral fellow in the group of Professor Matile at the University of Geneva, Switzerland. His research interests are centered around artificial photosynthesis.

Adam Sisson graduated MChem from the University of Sheffield (UK) in 2001. He gained a PhD from the University of Bristol (UK) in 2005, synthesising and studying steroid-derived receptors for anions as transmembrane transporters in the group of Professor Anthony Davis. His research interests are in supramolecular chemistry in lipid bilayers and he is currently pursuing these interests post-doctorally in the group of Professor Matile in Geneva.

Naomi Sakai gained her BS from Keio University (1987) and her PhD from Tokushima Bunri University (1994). After a post-doctoral stay in the group of Professor Koji Nakanishi at Columbia University (1994–1996), she focused on bioorganic biomembrane chemistry, first in Washington DC (Georgetown University, 1996–1999), then in Geneva (1999–present).

Stefan Matile received his Diploma (1989) and PhD (1994) from the University of Zurich under the direction of Professor Wolf Woggon. After a post-doc with Professor Koji Nakanishi at Columbia University, New York (1994–1996), and three years at Georgetown University, Washington DC, he moved to the University of Geneva (1999). His research interests are at the interface of synthetic organic, biological and supramolecular chemistry, where his current emphasis is on multifunctional nanoarchitecture in lipid bilayer membranes.

create function in lipid bilayer membranes. This new development is briefly described in the following sections.

2 Rosette receptors and ion channels

The programmed assembly of calix[4]arene dimelamines **3a** and barbiturates **4a** into double rosettes **5a** was found to occur in bilayer membranes (Fig. 2).[9] Namely, circular dichroism (CD) spectroscopy was used to demonstrate the formation of rosette **5a** in somewhat unusual bilayer vesicles composed of non-ionic polyoxyethylene alkyl ether surfactants. The perylenediimide in barbiturate **4a** was introduced for detectability by fluorescence microscopy only and was not expected to contribute to the π-stack architecture (*cf.* Sections 4 and 5).

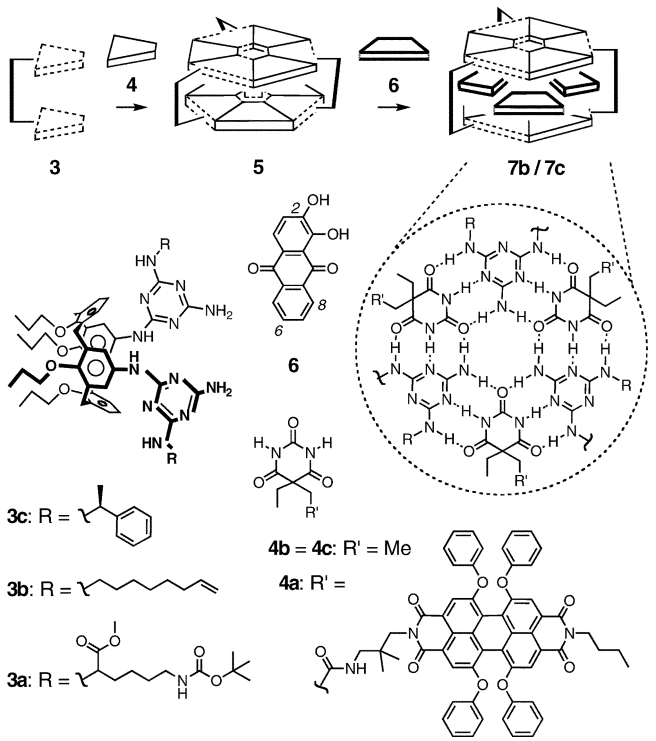

Fig. 2 Programmed assembly of double rosettes **5** from calix[4]arene dimelamines **3** and barbiturates **4**, and the formation of supramolecular host–guest complex **7** by intercalation of anthraquinone **6**.

The studies of π-stacked rosettes **5a** in bilayer membranes did not include function. The intercalation of guests such as **6** into nearly identical supramolecular hosts such as **5b** and **5c**, however, has been investigated in detail in organic solvents. The most recent highlight of a series of papers on this topic describes that the intercalation of anthraquinone **6** into the chiral rosette **5c** coincides with CD silencing.[10] This finding suggested that guest intercalation causes an untwisting of the staggered, helical conformation of host **5c** into the eclipsed conformation of complex **7c** (*cf.* Sections 3 and 5). X-Ray crystallography, NMR spectroscopy and successful cross-linking of staggered **5b** but not eclipsed **7b** by olefin metathesis confirmed the validity of this interpretation.

Extensive insights from isothermal titration calorimetry (ITC), absorption, CD and NMR titrations describe guest intercalation as enthalpy-driven, cooperative, and selective. Low dissociation constants around $K_D \approx 1$ nM increased rapidly with variation of the substitution pattern of the anthraquinone guest. Strongest destructive influences are observed with the removal of the hydroxy group in position 2 of **6**, engaged in a hydrogen-bonding network with neightboring guests, and addition of hydroxy groups in positions 6 and 8 that interfere with the calixarene cones.

In the presence of potassium cations, guanosines like **8** self-assemble into stacked rosettes like **9** (Fig. 3).[11] It was recognized early on that the central string of cations and the hydrophobic periphery of ionophoric rosettes such as the G-quartet stacks **9** are reminiscent of an ion channel. Stacked rosettes **9** exhibited ionophoric activity in bulk liquid membranes. In large unilamellar vesicles composed of egg yolk phosphatidylcholine (EYPC LUVs), however, guanosine **8** was inactive in all explored assays. Namely, inactivity was found in the HPTS assay, *i.e.* a fluorescence assay that monitors the velocity of the collapse of an applied proton gradient. Inactivity was also found in the Na NMR assay, an assay that follows the flux of sodium cations with the help of the membrane-impermeable NMR shift reagent dyprosium triphosphate.

These failures suggested that the templated self-assembly of guanosine **8** into ionophoric G-quartets **9** is unfavored in lipid bilayer membranes. To enforce the creation of G-quartet ion channels, a covalent capture strategy of the supramolecular rosette **9** was selected. Namely, ring-closing metathesis with Grubbs catalyst transformed supramolecule **9** into macromolecule **10**. Transport activity in EYPC LUVs in both the HPTS and Na NMR assay were in support of the formation of unimolecular ion channels by the cross-linked G-quartet **10**. The CD spectrum of **10** implied G-quartet formation in the presence but not in the absence of vesicles.

Compared to other ionophoric rosettes such as inactive G-quartets **9**, folate dendrimers **11** were particularly promising candidates to self-assemble into rosette ion channels **12** without being forced to do so by covalent capture (Fig. 4).[12] Folate quartets **12** can exist in hydrophobic media with and without central ion templates, and the H-bonded dendritic periphery may cushion[8] the dynamic rosette 'breathing' motions during ion hopping along the central string of ions.

Incorporation of dendrimers **11** into EYPC vesicles caused the appearance of the CD signature of stacked folate quartets **12**. Dendritic folate ion channels **12** showed activity in the HPTS assay (see above). Saturation behavior in the Hill plot was as expected for exergonic self-assembly of stacked rosettes **12**. It may further indicate poor partitioning into the bilayer. No activity was found for rosette **12** in the ANTS/DPX assay [*i.e.* a fluorescence assay that monitors the velocity of efflux of intravesicular molecules ANTS (an anionic fluorophore) or DPX (a cationic quencher)]. Activity in the pH-sensitive HPTS assay and inactivity in the ANTS/DPX assay was consistent with the small inner diameter expected for ion channel **12**.

In planar EYPC bilayers, the addition of dendrimers **11** caused the appearance of three dominant single-channel currents that were surprisingly homogeneous for a complex supramolecule such as **12**. The low conductance of 19 ± 2 (69%), 14 ± 2 (27%) and 7 ± 2 pS (14%) of these ohmic ion channels was consistent with the expected small inner diameter of folate quartets **12** ($d_{Hille} = 3.7$ Å). The anion/cation selectivity was significant (permeability ratio $P_{K^+}/P_{Cl^-} = 4.9$). The cation selectivity topology (Eisenmann I)

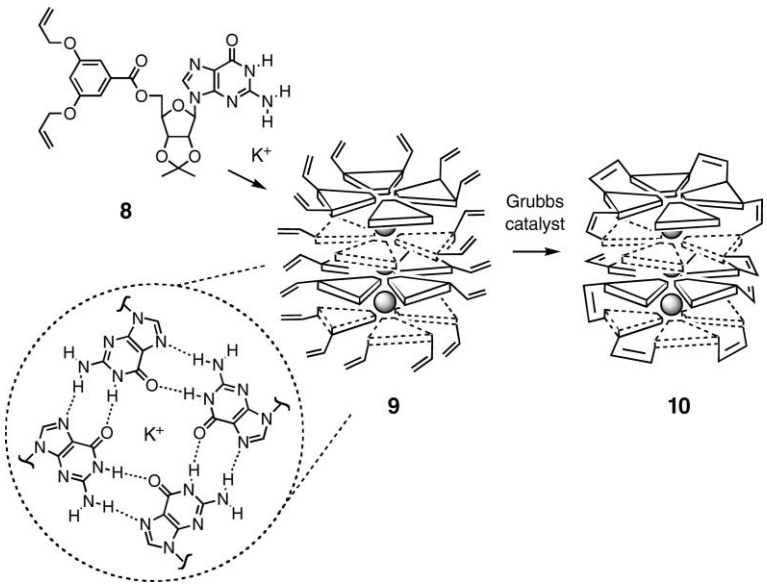

Fig. 3 Templated self-assembly of stacked G-quartets **9** from guanosines **8** in the presence of potassium cations and conversion into unimolecular ion channel **10** by ring-closing metathesis with Grubbs catalyst.

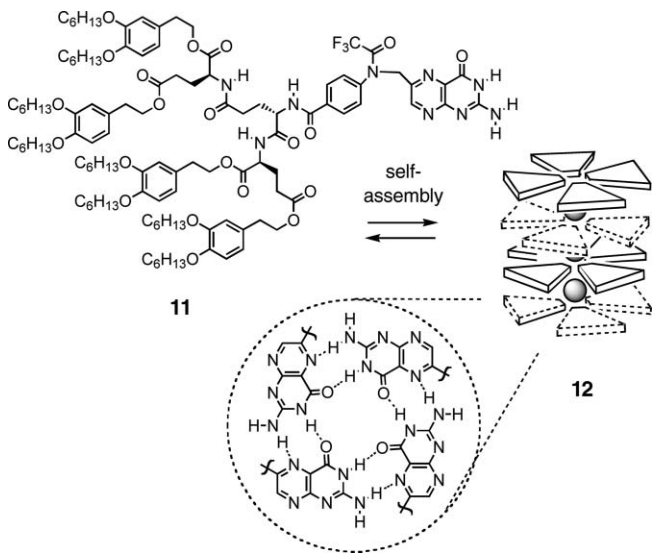

Fig. 4 Self-assembly of stacked folate quartets **12** from dendrimers **11**.

demonstrated dominance of cation dehydration as expected for the hopping of large ions through small holes along the central string of ions in stacked folate rosettes **12**. Blockage by the permeant cation confirmed the ionophoric properties of ion channel **12** [EC_{50} (K^+) = 230 mM, g_{MAX} = 21 pS].

3 Ligand-gated ion channels

To stop a process is always easier than to start one. In the field of synthetic ion channels and pores, this common wisdom is reflected in our inability to create synthetic ion channels and pores that open (ligand gating) rather than close (ligand blockage) in response to chemical stimulation. Rigid-rod π-stack barrel-stave architecture **13** was introduced last year to change this situation (Fig. 5).[13,14]

Ligand gating by aromatic electron donor–acceptor interactions was designed based on hoop–stave mismatch. The architecture of a barrel-stave ion channel requires approximate hydrophobic matching with regard to the surrounding membrane (2.5–3.5 nm) on the one hand and precise matching of the repeat distances in the stave with the repeat distances between the 'hoops' that hold the staves together. In the classical rigid-rod β-barrel **2**, for example, precise hoop–stave matching between phenyl repeats in the *p*-oligophenyl stave and the repeat distances in antiparallel β-sheets assures self-assembly of the barrel-stave supramolecule (Fig. 1).[8]

Self-assembly with hoop–stave mismatch produces helical rather than barrel-stave supramolecules. Replacement of the β-sheets in rigid-rod β-barrel **2** by π-stacks with shorter repeat distances should therefore result in a rigid-rod π-helix like **13** (rather than a holey rigid-rod π-barrel). The intercalation of ligands like **14** into the closed π-helix **13** should, however, reduce the hoop–stave mismatch and cause an untwisting helix–barrel transition to open up into a barrel-stave ion channel like **15**. Note the similarity of this approach with the untwisting of double rosette **5** in response to the intercalation of anthraquinone guests **6** (Fig. 2).

The validity of this adventurous concept was probed with electron-poor 1,4,5,8-naphthalenediimides (NDIs) to assure favorable self-assembly of monomeric *p*-octiphenyl rods **16** into π-helix **13**. Flanking H-bonded chains were added to orient the NDI stacks. Alkylammonium tails were introduced to secure the internal crowding and charge repulsion needed to stabilize higher oligomers.

Electron-rich 1,5-dialkoxynaphthalenes (DANs) as in ligand **14** and electron-poor NDIs as in helix **13** form plum-colored charge-transfer (CT) complexes (see Section 4). This aromatic electron donor–acceptor interaction was envisioned for the ligand-gated opening of closed π-helix **13** into barrel-stave ion channel **15**. A sulfonate was added at one side of ligand **14** to support the DAN–NDI CT complexes by ion pairing, an alkyl tail at the other for favorable interactions with the surrounding lipid bilayer membrane.

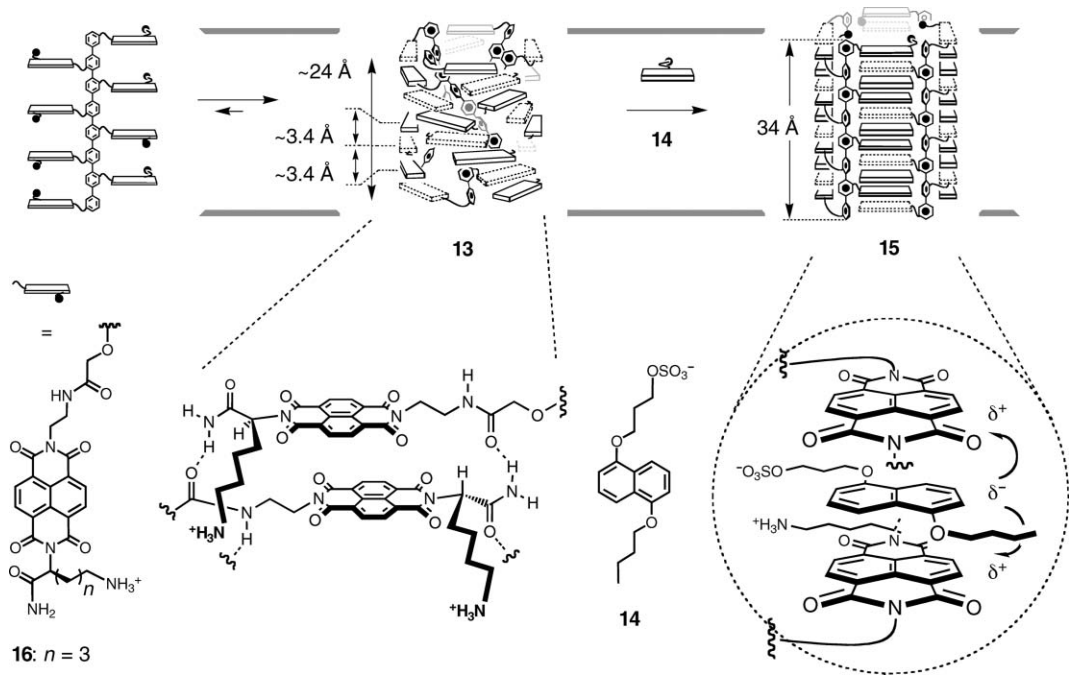

Fig. 5 Self-assembly of rigid-rod **16** into closed quadruple π-*M*-helix **13**, and helix–barrel transition into open ion channel **15** in response to the intercalation of ligands **14**.

In both planar and spherical EYPC bilayers, the closed channel **13** and ligand **14** were inactive. Mixed together, highly cooperative (n = 6.5, EC_{50} = 13 μM) intercalation of donors **14** caused the expected helix–barrel transition and produced surprisingly homogenous, ohmic, low-conductance (expected: $d \approx 5$ Å, found: d_{Hille} = 3.5 Å; g = 94 pS) anion channels **15** (P_{Cl^-}/P_{K^+} = 1.38). Shortening of the alkylammonium tails in channel **13** and removal of either anionic head or hydrophobic tail in ligand **14** all cleanly annihilated ligand-gated ion channel formation, and other intercalators such as adenosine 5′-monophosphate (AMP) or guanosine 5′-monophosphate (GMP) were inactive.

According to exciton-coupled CD of the twisted NDI stacks, π-*M*-helix **13** is reasonably stable toward chemical denaturation (guanidinium chloride, $-\Delta G^{H_2O} \approx 1.3$ kcal mol^{-1}) and is almost thermophilic compared to DNA duplexes ($T_M \geqslant 70$ °C). A helix–barrel transition as the origin of ligand gating was confirmed by silencing of the exciton-coupled CD signature of *M*-π-helix **13**. Operational aromatic donor–acceptor interactions were visible for the naked eye as plum color of ion channel **15** (*cf.* Section 5).

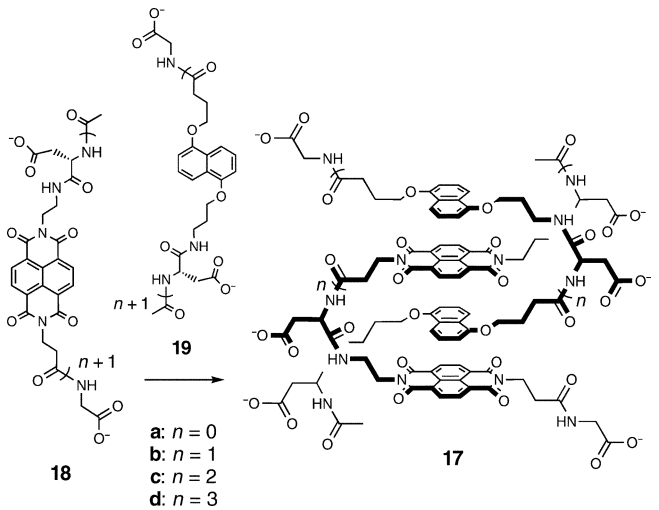

Fig. 6 Programmed assembly of duplexes **17** from oligo-NDI **18** and oligo-DAN **19** in water.

4 Architecture, conductivity and color

The use of 1,4,5,8-naphthalenediimides (NDIs) in transmembrane functional π-stack architecture such as ligand-gated ion channel **15** is attractive for three main reasons. Pertinent highlights concerning the architecture, conductivity and color of NDI are briefly summarized in this section.

Architecture

Two representative and pioneering examples out of a growing collection of refined NDI architecture are shown in Figs. 6 and 7. Oligomers with alternating DAN and NDI units were actually among the first foldamers characterized in neutral aqueous solution.[15] More recently, this approach was expanded to the programmed assembly of DAN–NDI duplexes **17** (Fig. 6).[16] The programmed assembly of oligo-NDI **18** and oligo-DAN **19** was characterized in neutral water. The dissociation constant (K_D) values decreased with increasing oligomer length to K_D = 29 μM for duplex **17d**. As in DNA duplexes, increasing repulsion of backbone charges in longer duplexes was seen not as a disadvantage but as an advantage to unfold single strands and to keep duplexes dissolved. The formation of duplexes **17d** was confirmed by gel electrophoresis. Recent developments in this research include elegant multiple intercalation of oligo-NDIs in DNA double helices.[17]

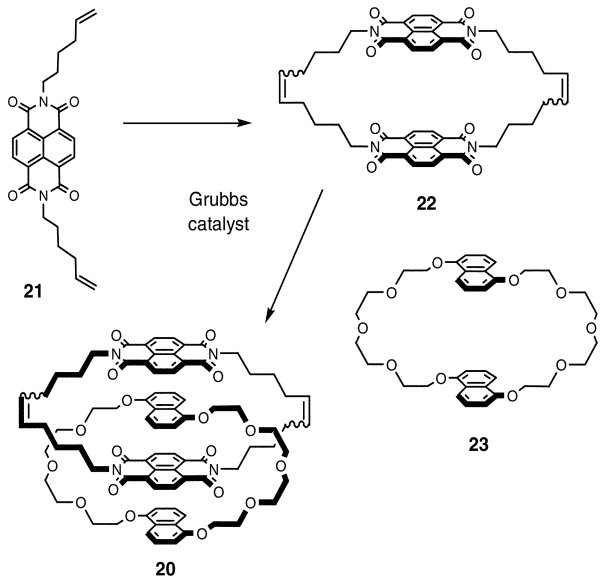

Fig. 7 Catenane **20** as another example for NDI acceptors in refined π-stack architecture created with aromatic donor–acceptor interactions.

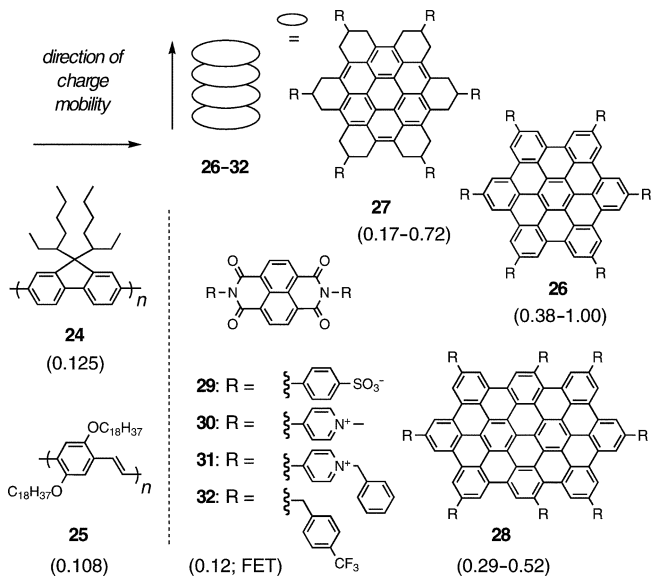

Fig. 8 Unidirectional charge mobilities in cm^2 $(Vs)^{-1}$ of some of the best p-conducting conjugated polymers (**24**, **25**) and π-stacks (**26**–**28**) and n-conducting NDI **32** measured under the unfavorable conditions common in field effect transistor (FET) research.

Catenane **20** is another example for pioneering supramolecular architecture accessible with the DAN–NDI motif (Fig. 7).[18] The preparation of catenane **20** combined aromatic donor–acceptor interactions with alkene metathesis (*cf.* Section 2, Figs. 2 and 3). Ring-closing metathesis of dialkene **21** produced NDI-macrocycle **22** in a mixture of products. In the presence of DAN-macrocycle **23**, catenane **20** was isolated as a mixture of *cis*/*trans* isomers in 50% yield. Recent developments in this research include ionophores,[19] rotaxanes and shuttles,[20,21] and gels.[22]

Conductivity

The conductivity of π-stack architecture is of the highest importance with regard to technological applications in molecular (opto)electronics.[23,24] The determinant parameter of organic semiconducting materials is the charge mobility. It determines, for example, the switching speed of field effect transistors (FETs), the intensity of light emitting diodes (LEDs), or the separation of charges in photovoltaic cells. In a recent overview, charge mobilities of π-stacked columnar discotic materials were compared with conjugated polymers.[24] In general, unidirectional charge mobilities are to a good part supramolecular parameters. With precise self-organization being as critical as monomer structure, charge mobilities naturally depend strongly upon sample conditions and history.

Values as large as 10 cm^2 $(Vs)^{-1}$ were reported for single-crystal polydiacetylenes that were polymerized in a controlled manner. Conjugated polymers with different backbones synthesized in solution gave two orders of magnitude lower values in the range of 0.009–0.125 cm^2 $(Vs)^{-1}$. Best mobilities in this series, around 0.1 cm^2 $(Vs)^{-1}$, were reported for liquid crystalline polyfluorene **24** and poly(phenylenevinylene) **25** (Fig. 8). Discotic liquid crystalline π-stacks gave clearly larger mobilities of up to 1 cm^2 $(Vs)^{-1}$ in crystalline and liquid crystalline phases. Compared to conjugated polymers, self-organization in refined π-stack architecture therefore can overcompensate the weaker electronic coupling between monomer units. Maximal mobilities found for intermediate-sized oligoarene **26** rather than the contracted coronene **27** or the expanded **28** were explained by gradual overcompensation of increasing π–π overlap with increasing core size. High mobilities were also found for π-stacked porphyrins and phthalocyanines. Recent highlights in this research include synthetic access to π-stacked coronene nanotubes.[25] For extensive research on the semiconducting properties of the π-stacks in DNA duplexes, the interested reader is referred to pertinent recent literature.[26,27]

Indications for conductive NDI stacks were observed early on with the appearance of a strong NIR-band at 1140 nm in response to electrochemical or chemical one-electron reduction of NDI **29** in water (Fig. 8).[28] This band was interpreted as a CT-band of π-dimers of the radical anion of **29**. Disappearance of the CT-band in less polar solvents like DMF was consistent with π-dimer disassembly. Just as for intramolecular delocalization in ordinary π-systems such as polyenes, it is expected that the delocalization length will determine the wavelength of absorption. Increasing intensity and bathochromic shift implied, therefore, self-assembly of π-dimers into NDI π-stacks with increasing ionic strength. The presence of NDI π-stacks of radical anion **29** in aqueous solution was supported by weak and anisotropic EPR signals similar to those found in the solid state. Reduced charge repulsion in the π-stacks of the radical anion of cationic NDI **30** was reflected in a bathochromic shift of the CT-band to 1700 nm. Increasing hydrophobicity of NDI **31** further stabilized the π-stack (2050 nm), and programmed assembly of anionic NDI **29** and cationic NDI **30** yielded mixed π-stacks.

The discovery of π-stacks of NDI radical anions was significant because, different from hole, positive or p-conducting polymers or π-stacks (*e.g.* **24**–**28**), electron, negative or n-conducting π-stacks or polymers are usually not air-stable. Precipitated films of the electrophores **29** were air-stable. The casting of NDI films in polymers [*e.g.* polyvinyl alcohol (PVA)] produced conductors with high anisotropy, sensitivity to humidity and the highest conductance with mixed valence π-stacks containing both neutral

and anionic NDIs. A more recent systematic search for maximal FET charge mobilities of NDI films yielded the best results for analog **32**.[29,30] The value of 0.12 cm^2 $(Vs)^{-1}$ found was clearly better than that of the most useful air-stable electron-carrying n-semiconductor [perfluorinated copper phthalocyanine, $\leqslant 0.02$ cm^2 $(Vs)^{-1}$]. The combination of NDIs as unique, air-stable and high-mobility n-channel organic semiconductors with unproblematic p-channel FETs was used to create complementary inverter circuits.

Color

The disappointing optical properties of Vollmann *et al.*'s early NDIs with arylamino core substituents may be the reason why core-substituted NDIs have never been really studied.[31] This situation changed dramatically with the introduction of alkylamino and alkoxy core substitution accomplished by the Wurthner group in 2002 (Fig. 9).[32] Pyrene **33** was converted into anhydride **34** in four steps following previously reported procedures. The conversion of dianhydride **34** into diimide **35** was achieved in 44% yield in acetic acid at 120 °C. Core substitution with *n*-butylamine at 85 °C gave the core-substituted *N*,*N*-NDI **36** in 45% yield. The core-substituted *O*,*O*-NDI **37** was prepared in 51% yield by treating **35** with sodium ethanolate at room temperature. Partial nucleophilic aromatic substitution of **35** with sodium ethanolate at room temperature (46%) followed by treatment with *n*-butylamine at 0 °C (47%) finally established the asymmetric core-substitution in *N*,*O*-NDI **38**.

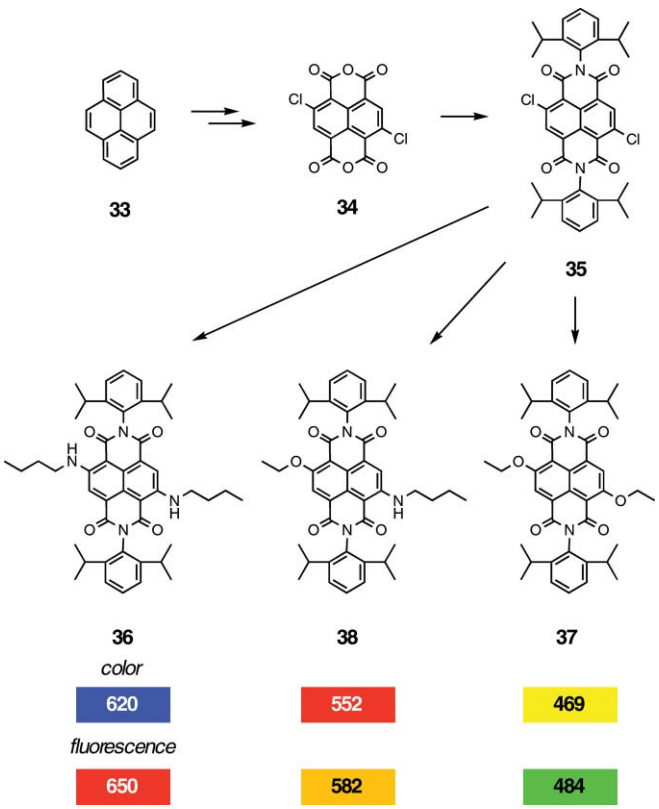

Fig. 9 Synthesis and spectroscopic properties of core-substituted naphthalenediimides (NDIs). Numbers in colored boxes refer to the wavelength of maximal absorption or emission (in nm).

In striking contrast to arylamino core substitution, brilliant colors and intense fluorescence were found with alkylamino and alkoxy core substituents. Introduction of the weaker alkoxy π-donors converted the colorless NDI into the yellow, green-fluorescent *O*,*O*-NDI **37**. Stronger alkylamino π-donors resulted in a red color and orange fluorescence for *N*,*O*-NDI **38** as well as the blue color and red fluorescence for *N*,*N*-NDI **36**. The redox potentials decreased correspondingly. Quantum yields of up to 76% were reported, increasing with decreasing solvent polarity. Important with regard to supramolecular architecture and different from core-substituted PDIs, X-ray structures confirmed that core-substituted NDIs are planar.

Core-substituted 3,4,9,10-perylenediimides (PDIs) are among the best studied and most promising chromophores with regard to technological applications in molecular (opto)electronics. In a milestone paper in 2002, the Wasielewski group reported that the enforced co-facial π-stacking in dimer **39** provides access to characteristics reminiscent of the special pair of chlorophylls in biological photosystems, *i.e.* excited-state symmetry breaking and ultrafast charge separation (Fig. 10).[33] Charge separation was studied following the transient absorption of the radical anion at 710–800 nm after excitation with an 80 fs laser flash at 400 nm. The transient absorption spectrum of co-facial dimer **39** was nearly identical with the spectroelectrochemically simulated spectrum of the radical ion pair. In toluene, charge separation occurred with $\tau_{CS} = 0.52$ ps, and recombination with $\tau_{RC} = 222$ ps; in 2-methyltetrahydrofuran (MTHF) with $\tau_{CS} = 0.33$ ps and $\tau_{RC} = 38$ ps. The linear dimer **40** showed no charge separation in toluene, and solvent dipole fluctuations are thought to account for the detectability of the much slower charge separation in the more polar MTHF ($\tau_{CS} = 55$ ps, $\tau_{RC} = 99$ ps). No charge separation was observed with monomeric controls. These findings established a firm relation between co-facial π-stacking in the PDI architecture and ultrafast charge separation. The presence and extent of the former turned out to be readily detectable from a bathochromic exciton transition at 632 nm in the absorption spectrum.

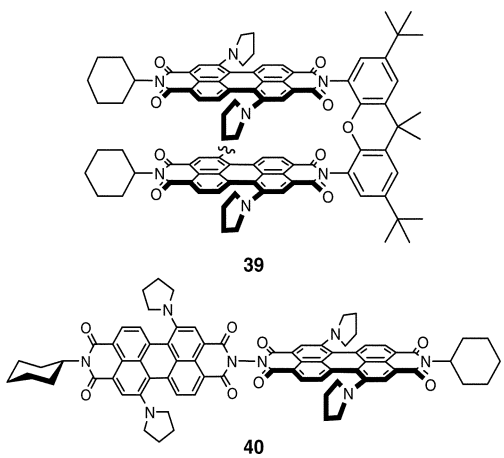

Fig. 10 The co-facial PDI dimer **39**, but not the linear PDI dimer **40**, is a chlorophyll special-pair mimic.

More recent highlights in this research include enforced co-facial PDI stacking in more complex as well as multichromophoric nanoarchitectures.[34,35] The need to artificially enforce co-facial stacking stems from the non-planarity of core-substituted PDIs.

One important difference of core-substituted NDIs compared to the otherwise perfect PDIs is their planarity. This planarity can be expected to maximize co-facial π-stacking and therefore, according to chlorophyll special-pair mimic **39**, maximize the charge separation in a photoactive nanoarchitecture.

5 Photosystems

Unimolecular photosystems

The state-of-the-art on artificial photosystems in bilayer membranes remains the carotenoid–porphyrin–quinone (C–P–Q) triad **41** (Fig. 11).[5,36] The terminal carboxylate is placed to control vectorial partitioning of the C–P–Q triad **41** into bilayer membranes, with the hydrophobic carotenoid donor located in the inner leaflet and the quinone acceptor in the outer leaflet. Quinone carrier Q_S **42** is made to have a higher reduction potential than the quinone in the C–P–Q triad **41** and to accumulate in the hydrophobic core of the membrane.

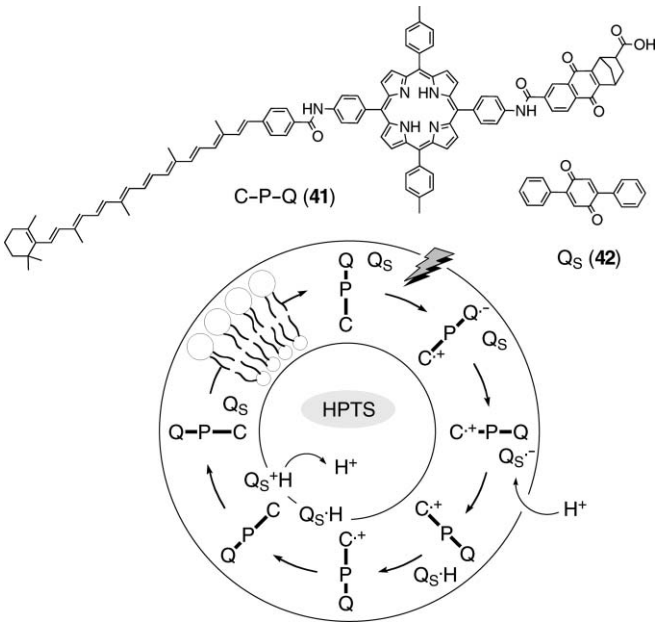

Fig. 11 Carotenoid–porphyrin–quinone triad **41** as a unimolecular photosystem, serving in the shown application together with quinone carrier **42** to pump protons with light across lipid bilayer membranes. The fluorophore HPTS is used to measure intravesicular acidification with light.

Extensive photophysical details are available to describe intramolecular charge separation in response to the excitation of the porphyrin in the C–P–Q triad **41**. The quinone radical anion of the charge-separated $C^{\bullet+}$–P–$Q^{\bullet-}$ triad then reduces a quinone Q_S near the outer membrane–water interface. The resulting semiquinone radical anion $Q_S^{\bullet-}$ is basic enough to accept a proton from the external aqueous environment. The neutral radical $HQ_S^{\bullet}$ is sufficiently lipophilic to diffuse across the bilayer and reduce the carotenoid radical cation near the inner membrane–water interface. The produced protonated HQ_S is a strong acid ($pK_a \approx -6$) that releases its proton internally. The overall result is the transport of a proton into a vesicle in response to light. This decrease in intravesicular pH could be readily measured with an entrapped pH-sensitive fluorescent probe (HPTS, 8-hydroxy-1,3,6-pyrenetrisulfonate). The maximal proton gradient of $\Delta pH \approx 2$ was stable for at least 4 h but could be readily collapsed by the addition of a proton carrier (FCCP). Because the proton pumping photocycle occurs without charge neutralizing co-transport, a transmembrane electrical potential builds up simultaneously. This photoinduced vesicle polarization was confirmed with a potentially sensitive fluorescent probe (8-anilino-1-naphthalenesulfonate). Vesicle depolarization by valinomycin-mediated potassium efflux resulted in the expected increase of the maximal proton gradient by $\Delta pH \approx 1.6$.

Extensive elegant follow up studies demonstrated that photosystem **41** can be coupled with ATP synthase to produce ATP from ADP with light,[37] adaptability to active calcium transport,[38] as well as tolerance toward significant structural modifications (*e.g.* fullerenes instead of quinones as acceptors).[5] Building on previous breakthroughs on electroneutral pyrylium electron carriers,[39] alternative recent approaches to photoinduced transmembrane charge separation focus on intermolecular electron transfer from excited porphyrin monomers in the water to photoregulated spiropyrane–anthraquinone electron carriers in the membrane.[40]

Photosystems with π-stack architecture

The inspiring recent breakthroughs in NDI and PDI chemistry summarized in the preceding sub-sections suggested that the sum of unique characteristics covering supramolecular architecture, conductivity and rainbow coloration may offer all that is needed to create photoactive π-stack nanoarchitectures. The blue-colored, red-fluorescent rigid-rod π-*M*-helix **43** was introduced this year to tackle this challenge (Fig. 12).[41]

On the structural level, the difference between the artificial photosystem **43** and the above closed ion channel **13** (Section 3, Fig. 5) is minimal: small isopropylamino π-donors are added to the NDI core. This small change in structure had little influence on the characteristics of the above rigid-rod π-*M*-helix **13**. Intercalation of ligands **14** into π-*M*-helices **43** caused the same CD-silencing helix–barrel transition and afforded active barrel-stave ion channels **44**.

However, the *N*,*N*-NDI core substitution of helix **43** did cause some remarkable changes compared to the colorless helix **13**. A clearly more demanding synthesis was rewarded with the appearance of the expected brilliant blue color and red fluorescence (the corresponding *N*,*N*-PDI control did not fluoresce). Dependence of activity and suprastructure on the fourth power of the concentration of monomer **45** demonstrated that photosystem **43** is a quadruple helix (Fig. 13). Extensive exciton coupling in the CD spectrum demonstrated *M*-helicity as well as self-assembly into the highly ordered nanoarchitecture required for satisfactory optoelectric properties (*cf.* Section 4). The appearance of a bathochromic exciton transition at 598 nm in the absorption spectrum implied the co-facial *N*,*N*-NDI-stacking in the *M*-helix **43** required for ultrafast charge separation (*cf.* above PDI dimers **39** and **40**, Fig. 10; this band was weaker or missing in shorter *N*,*N*-NDI controls like **46**).

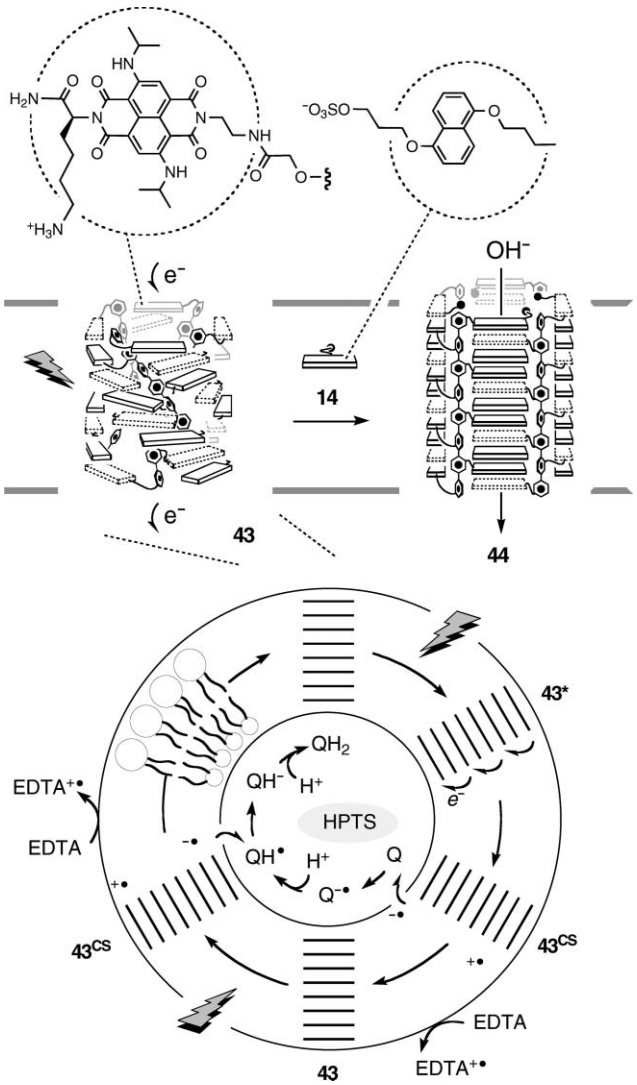

Fig. 12 Quadruple rigid-rod π-*M*-helix **43** as a supramolecular photosystem that can open up into ion channel **44**. In the shown application, transmembrane photoinduced electron transfer from EDTA donors to quinone acceptors Q is measured as formal proton pumping with light across lipid bilayers. HPTS is used to measure intravesicular deacidification with light (*cf.* Fig. 13).

Photosystem **43** (Fig. 12) was characterized in vesicles equipped with external electron donors (EDTA, ethylenediaminetetraacetate), internal electron acceptors (Q, 1,4-naphthoquinone-2-sulfonate), and an internal fluorescent pH meter (HPTS). In this system, transmembrane charge separation $\mathbf{43}^{CS}$ in response to the irradiation of helix **43** is translated into external EDTA oxidation [$E_{1/2}$ (NHE) ≈ +430 mV] and internal quinone reduction [$E_{1/2}$ (NHE) ≈ −60 mV] for the fluorometric detection of photoactivity as intravesicular deacidification with light. Thermally unfavorable by $\Delta E \approx 0.5$ V, this experimentally observed photoreduction occurs therefore by partial conversion of photonic energy into chemical energy (Fig. 13).

The addition of ligand **14** caused immediate collapse of the proton gradient created with light and photosystem **43**. This finding was consistent with smart supramolecular architecture, *i.e.* the programmed transition from active electron transport with photosystem **43** to passive anion transport with ion channel **44** in response to chemical stimulation with ligand **14**. Intercalator **14** naturally inhibited photosystem **43**.

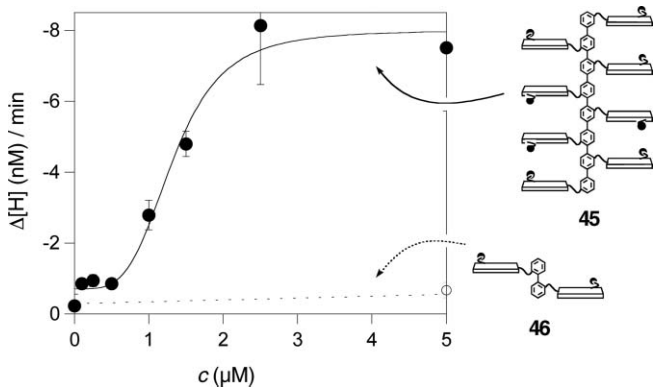

Fig. 13 Initial velocity of intravesicular proton consumption during irradiation at 640 nm as a function of the concentration *N*,*N*-NDI octamer **45** and *N*,*N*-NDI dimer **46** (*cf.* Fig. 12). The Hill coefficient $n = 3.9$ (solid line) indicates self-assembly of monomer **45** into the photoactive quadruple rigid-rod π-*M*-helix **43**. Data adapted from ref. 41. © American Association for the Advancement of Science, 2006.

The activity of photosystem **43** was perfectly reflected in nearly quantitative ultrafast formation (<2 ps, >97%) and a long lifetime of the charge-separated state $\mathbf{43}^{CS}$ (61 ps). The optical signature of this crucial $\mathbf{43}^{CS}$ was identified with the appearance of a new band at 480–540 nm in the transient absorption spectrum of a monomeric *N*,*N*-NDI in the presence of an electron donor (DMA, *N*,*N*-dimethylaniline). Stabilization of the radical cation *N*,*N*-NDI$^{+\bullet}$ with acceptor TCNE (tetracyanoethylene) was not detectable. The transient *N*,*N*-NDI$^{-\bullet}$ band of photosystem **43** was, therefore, used to characterize the charge-separated state $\mathbf{43}^{CS}$.

The disappearance of activity upon shortening of the rigid-rod scaffold in *N*,*N*-NDI biphenyl **46** did coincide with the disappearance of indications for (a) self-organization in the CD spectrum and (b) co-facial π-stacking in the absorption spectrum. Chromophore expansion to *N*,*N*-PDI as in Fig. 10 gave poor photoactivity, independent of the length of the *p*-oligophenyl rods used. Poor co-facial π-stacking in the absorption spectrum indicated that insufficient π-architecture accounts for the remarkably poor photoactivity of chromophores with perfect optoelectric properties (*cf.* Section 4). Reduced activity of these control molecules with a varied rod or chromophore length provided experimental evidence that it is neither the number nor the nature of the chromophores but the multifunctional supramolecular π-architecture that accounts for the superb activity of photosystem **43**.

6 Perspectives

Over a short period of time, several design strategies for the creation of functional π-stack architectures in bilayer membranes have emerged. This includes the formation of ion channels by stacked rosettes such as guanine or folate quartets. Ion channels that open up in response to chemical stimulation, *i.e.* ligand gating, became available with the introduction of aromatic electron donor–acceptor interactions between naphthalenediimide (NDI) acceptors and dialkoxynaphthalene (DAN) donors in rigid-rod π-stack architectures. Similar untwisting found for stacked

melamine–barbiturate rosettes in response to anthraquinone intercalation may illustrate the attractive scope of this approach.

The distinguishing characteristics of π-stack architecture, however, are conductivity and color, with charge mobilities depending critically upon the precision of the supramolecular organization. The usefulness of these characteristics to create function in lipid bilayer membranes was confirmed with the synthesis of smart photosystems that can switch from active electron transport to passive ion transport in response to chemical stimulation.

Synthetic access to functional π-stack architecture in lipid bilayer membranes may open several doors. It offers an innovative approach to new synthetic ion channels and pores with practical applications as detectors, sensors, catalysts or drugs.[6,7] Experimental evidence for π-stack architecture as a privileged platform to create smart photosystems in lipid bilayer membranes is particularly stimulating. Synthetic efforts toward asymmetric rigid-rod push–pull[42] π-stack architecture to orient[43] and stabilize charge separation, and toward transmembrane traffic lights with *N*,*N*-, *N*,*O*-, *O*,*O*-NDI fluorophores (Fig. 9) to harvest light, are on-going. Vesicle polarization[44] for voltage gating and coupling of smart photosystems with catalyst cascades to, perhaps, split water[4,45–47] with light in bilayer membranes are other attractive but challenging topics under investigation. Although the suggested usefulness in solar cells and related devices such as solar-based biofuel cells remains questionable, there is progress made to stabilize lipid bilayer membranes by, *e.g.* vesicle encapsulation in silica-gel matrices.[48] Research on functional π-stack architecture in bilayer membranes will in any case contribute to the major effort in basic research on smart optoelectric nanomaterials that is, according to pertinent reports,[49] needed today to meet tomorrow's energy demands in a sustainable way.

Acknowledgements

We thank the Swiss NSF for financial support. S. B. is a fellow of the Roche Research Foundation.

References

1 J. Deisenhofer and H. Michel, *Science*, 1989, **245**, 1463–1473.
2 N. Nelson and A. Ben-Shem, *Nat. Rev. Mol. Cell Biol.*, 2004, **5**, 971–982.
3 P. Jordan, P. Fromme, H.-T. Witt, O. Klukas, W. Saenger and N. Krauss, *Nature*, 2001, **411**, 909–917.
4 J. N. Robinson and D. J. Cole-Hamilton, *Chem. Soc. Rev.*, 1991, **20**, 49–94.
5 D. Gust, T. A. Moore and A. L. Moore, *Acc. Chem. Res.*, 2001, **34**, 40–48.
6 S. Matile, A. Som and N. Sordé, *Tetrahedron*, 2004, **60**, 6405–6435.
7 A. L. Sisson, M. R. Shah, S. Bhosale and S. Matile, *Chem. Soc. Rev.*, 2006, DOI: 10.1039/b512423a.
8 N. Sakai, J. Mareda and S. Matile, *Acc. Chem. Res.*, 2005, **38**, 79–87.
9 M. G. ten Cate, M. Crego-Calama and D. N. Reinhoudt, *J. Am. Chem. Soc.*, 2004, **126**, 10840–10841.
10 J. M. Kerckhoffs, M. G. ten Cate, M. A. Mateos-Timoneda, F. W. van Leeuwen, B. Snellink-Ruel, A. L. Spek, H. Kooijman, M. Crego-Calama and D. N. Reinhoudt, *J. Am. Chem. Soc.*, 2005, **127**, 12697–12708.
11 M. S. Kaucher, W. A. Harrell, Jr. and J. T. Davis, *J. Am. Chem. Soc.*, 2006, **128**, 38–39.
12 N. Sakai, Y. Kamikawa, M. Nishii, T. Matsuoka, T. Kato and S. Matile, *J. Am. Chem. Soc.*, 2006, **128**, 2218–2219.
13 P. Talukdar, G. Bollot, J. Mareda, N. Sakai and S. Matile, *J. Am. Chem. Soc.*, 2005, **127**, 6528–6529.
14 P. Talukdar, G. Bollot, J. Mareda, N. Sakai and S. Matile, *Chem.–Eur. J.*, 2005, **11**, 6525–6532.
15 R. S. Lokey and B. L. Iverson, *Nature*, 1995, **375**, 303–305.
16 G. J. Gabriel and B. L. Iverson, *J. Am. Chem. Soc.*, 2002, **124**, 15174–15175.
17 J. Lee, V. Guelev, S. Sorey, D. W. Hoffman and B. L. Iverson, *J. Am. Chem. Soc.*, 2004, **126**, 14036–14042.
18 D. G. Hamilton, N. Feeder, S. J. Teat and J. K. M. Sanders, *New J. Chem.*, 1998, **22**, 1019–1021.
19 G. Kaiser, T. Jarrosson, S. Otto, Y. F. Ng, A. D. Bond and J. K. M. Sanders, *Angew. Chem., Int. Ed.*, 2004, **43**, 1959–1962.
20 S. A. Vignon, T. Jarrosson, T. Iijima, H. R. Tseng, J. K. M. Sanders and J. F. Stoddart, *J. Am. Chem. Soc.*, 2004, **126**, 9884–9885.
21 T. Iijima, S. A. Vignon, H. R. Tseng, T. Jarrosson, J. K. M. Sanders, F. Marchioni, M. Venturi, E. Apostoli, V. Balzani and J. F. Stoddart, *Chem.–Eur. J.*, 2004, **10**, 6375–6392.
22 P. Mukhopadhyay, Y. Iwashita, M. Shirakawa, S. Kawano, N. Fujita and S. Shinkai, *Angew. Chem.,Int. Ed.*, 2006, **45**, 1592–2595.
23 F. J. M. Hoeben, P. Jonkheijm, E. W. Meijer and A. P. H. J. Schenning, *Chem. Rev.*, 2005, **105**, 1491–1546.
24 J. M. Warman, M. P. de Haas, G. Dicker, F. C. Grozema, J. Piris and M. G. Debije, *Chem. Mater.*, 2004, **16**, 4600–4609.
25 J. P. Hill, W. Jin, A. Kosaka, T. Fukushima, H. Ichihara, T. Shimomura, K. Ito, T. Hashizume, N. Ishii and T. Aida, *Science*, 2004, **304**, 1481–1483.
26 C. Wan, T. Fiebig, O. Schiemann, J. K. Barton and A. H. Zewail, *Proc. Natl. Acad. Sci. U. S. A.*, 2000, **97**, 14052–14055.
27 B. Giese, *Curr. Opin. Chem. Biol.*, 2002, **6**, 612–618.
28 L. L. Miller and K. R. Mann, *Acc. Chem. Res.*, 1996, **29**, 417–423.
29 H. E. Katz, A. J. Lovinger, J. Johnson, C. Kloc, T. Siegrist, W. Li, Y. Y. Lin and A. Dodabalapur, *Nature*, 2000, **404**, 478–481.
30 H. E. Katz, J. Johnson, A. J. Lovinger and W. Li, *J. Am. Chem. Soc.*, 2000, **122**, 7787–7792.
31 H. Vollmann, H. Becker, M. Corell and H. Streeck, *Liebigs Ann. Chem.*, 1937, **531**, 1–159.
32 F. Wurthner, S. Ahmed, C. Thalacker and T. Debaerdemaeker, *Chem.–Eur. J.*, 2002, **8**, 4742–4750.
33 J. M. Giaimo, A. V. Gusev and M. R. Wasielewski, *J. Am. Chem. Soc.*, 2002, **124**, 8530–8231.
34 B. Rybtchinski, L. E. Sinks and M. R. Wasielewski, *J. Am. Chem. Soc.*, 2004, **126**, 12268–12269.
35 M. J. Ahrens, L. E. Sinks, B. Rybtchinski, W. Liu, B. A. Jones, J. M. Giaimo, A. V. Gusev, A. J. Goshe, D. M. Tiede and M. R. Wasielewski, *J. Am. Chem. Soc.*, 2004, **126**, 8284–8294.
36 G. Steinberg-Yfrach, P. A. Liddell, S.-C. Hung, A. L. Moore, D. Gust and T. A. Moore, *Nature*, 1997, **385**, 239–241.
37 G. Steinberg-Yfrach, J. L. Rigaud, E. N. Durantini, A. L. Moore, D. Gust and T. A. Moore, *Nature*, 1998, **392**, 479–482.
38 I. M. Bennett, H. M. Farfano, F. Bogani, A. Primak, P. A. Liddell, L. Otero, L. Sereno, J. J. Silber, A. L. Moore, T. A. Moore and D. Gust, *Nature*, 2002, **420**, 398–401.
39 R. F. Khairutdinov and J. K. Hurst, *Nature*, 1999, **402**, 509–511.
40 L. Zhu, R. F. Kairutdinov, J. L. Cape and J. K. Hurst, *J. Am. Chem. Soc.*, 2006, **128**, 825–835.
41 S. Bhosale, A. L. Sisson, P. Talukdar, A. Fürstenberg, N. Banerji, E. Vauthey, G. Bollot, J. Mareda, C. Röger, F. Würthner, N. Sakai and S. Matile, *Science*, 2006, **313**, 84–86.
42 N. Sakai and S. Matile, *J. Am. Chem. Soc.*, 2002, **124**, 1184–1185.
43 S. Yasutomi, T. Morita, Y. Imanishi and S. Kimura, *Science*, 2004, **304**, 1944–1947.
44 N. Sakai and S. Matile, *Chem. Biodiversity*, 2004, **1**, 28–43.
45 D. L. Jiang, C. K. Choi, K. Honda, W. S. Li, T. Yuzawa and T. Aida, *J. Am. Chem. Soc.*, 2004, **126**, 12084–12089.
46 L. Sun, L. Hammarström, B. Åkermark and S. Styring, *Chem. Soc. Rev.*, 2001, **30**, 36–49.
47 W. Rüttinger and C. G. Dismukes, *Chem. Rev.*, 1997, **97**, 1–24.
48 T.-J. M. Luo, R. Soong, E. Lan, B. Dunn and C. Montemagno, *Nat. Mater.*, 2005, **4**, 220–224.
49 *Basic Research Needs for Solar Energy Utilization*, US Department of Energy, 2005, http://www.sc.doe.gov/bes/reports/files/SEU_rpt.pdf; G. Hess, *Chem. Eng. News*, 2005, **83**(34), 12.